

Measurement of the motional heating of a levitated nanoparticle by thermal lightA. T. M. Anishur Rahman^{✉*} and P. F. Barker[†]*Department of Physics & Astronomy, University College London, London WC1E 6BT, United Kingdom* (Received 11 May 2022; revised 7 September 2022; accepted 3 January 2023; published 24 January 2023)

We report on measurements of the photon-induced heating of silica nanospheres levitated in a vacuum by a thermal light source formed by a superluminescent diode. Heating of the nanospheres motion along the three trap axes was measured as a function of gas pressure for two particle sizes and recoil heating was shown to dominate other heating mechanisms due to relative intensity noise and beam pointing fluctuations. Heating rates were also compared with the much lower reheating of the same sphere when levitated by a laser.

DOI: [10.1103/PhysRevA.107.013521](https://doi.org/10.1103/PhysRevA.107.013521)**I. INTRODUCTION**

Optomechanical interactions are routinely used to cool and control the motion of mechanical objects including those in gravitational wave detection [1] and levitated optomechanics [2]. The effectiveness of such interactions are, however, eventually limited by the discrete nature of the light. For example, fluctuations in the photon number lead to measurement noise and recoil heating [3–6]. However, the optomechanical effects of squeezed light, Bose-Einstein condensate of photons [7,8], or the light of different photon statistics such as the Bose-Einstein (BE) on levitated systems have not been explored experimentally yet, although squeezed light sources have now been proposed for reducing the recoil heating of such oscillators [9].

Recently, we demonstrated the trapping of nanoparticles with thermal light from a superluminescent diode (SLD) [10]. The broadband nature of this source allows spectral shaping of the output profile which can be used to create arbitrary optical potentials. SLDs have also found applications in cold atoms in places of lasers with potential use in atomtronics and quantum simulation [11]. The low temporal coherence time and the BE photon statistics of such light sources closely resemble that of a blackbody (BB) source [12–14]. However, unlike a BB source, a SLD has a high spatial coherence with a well-defined polarization [15] allowing it to be tightly focused and used for optical trapping [10]. Moreover, as this light is of thermal nature, the motional temperature of any object levitated by such light should, in the absence of other noise, equilibrate to the temperature of the light source as originally envisioned by Einstein [16].

We report on the measurement of the heating of a nanomechanical oscillator in a high vacuum when levitated using thermal light obtained from a SLD. In particular, we confirm the enhanced heating of the levitated oscillator expected

from such a source when compared with the same oscillator levitated by a laser. We also describe the measurement of the direction-dependent heating along all three translational axes of the levitated nanoparticle. We compare this with the heating rates expected from both relative intensity noise and beam pointing instabilities and confirm that the recoil heating from thermal photons dominates all other heating mechanisms present in our optical trap.

II. EXPERIMENT

To measure the heating of the levitated particle by the thermal light from the SLD and a laser we create an optical tweezer by focusing either beam using the same high numerical aperture lens ($NA = 0.77$) [Fig. 1(a)]. The laser operates at a wavelength of 1064 nm, while the superluminescent diode is centered around 1060 nm. We trap a silica nanoparticle using one of the beams and then transfer it to the other trapping beam when required [10]. At any time only one beam is used. The spectral intensity profiles of our SLD and the laser are shown in Fig. 1(b).

III. THEORETICAL MODEL

The thermal light from the SLD is amplified spontaneous emission and its photon statistics follow the BE distribution [14,17]. In a BE distribution [12,18,19] the average and the variance of the photon number are $\bar{n} = \frac{1}{\exp[(\hbar\omega - \mu_c)/k_B T] - 1}$ and $\Delta n^2 = \bar{n} + \bar{n}^2$, where ω and c are the angular frequency and the speed of light, k_B is the Boltzmann constant, T is the bulk temperature of the light source, and μ_c is the chemical potential or the band gap of the underlying p - n junction. Thermal light contains many modes with a mode density $M_d = \frac{\omega^2}{\pi^2 c^3}$ [18]. The average number of photon emitted in a mode per second by a SLD of optical gain $G(\omega)$ and a p - n junction of area A_{pn} is $G(\omega)A_{pn}cM_d\bar{n}$. The output power in a mode is $\frac{GA_{pn}}{\pi^2 c^2} \frac{\hbar\omega^3}{\exp[(\hbar\omega - \mu_c)/k_B T] - 1}$. When $G(\omega) = 1$ and $A_{pn} = 1 \text{ m}^2$ and $\mu_c = 0$, one recovers the usual blackbody spectrum [12,18].

*Present address: Department of Physics, University of Warwick, Coventry CV4 7AL, UK; a.rahman@ucl.ac.uk

†p.barker@ucl.ac.uk

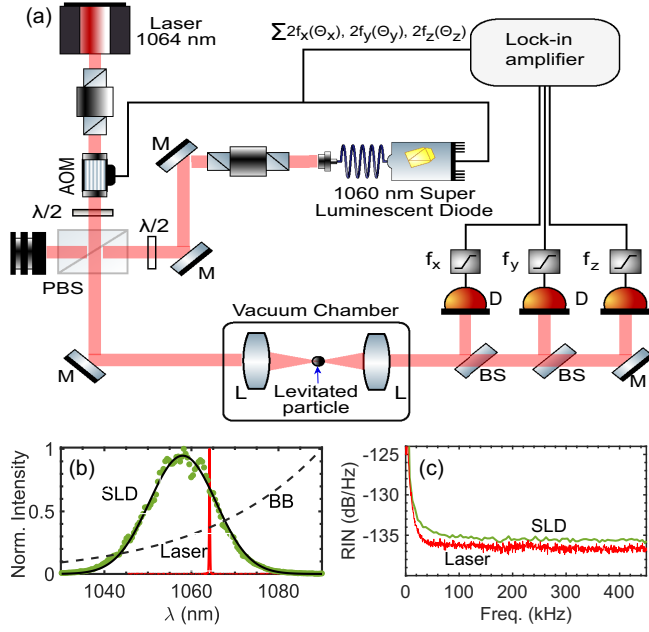


FIG. 1. (a) A schematic of our experimental setup in which a particle can be levitated and parametrically cooled using a laser beam or the light from a superluminescent diode. Different components are as follows: D is balanced photodiode, M represents the mirror, BS the beam splitter, L the lens, PBS is the polarizing beam splitter, and $\lambda/2$ the half wave plate. (b) Normalized spectral intensity profiles of the superluminescent diode, a single longitudinal mode laser, and an ideal blackbody source at $T = 295$ K. The spectral profile of the SLD is fitted with a Gaussian (black solid line). (c) Relative intensity noise (RIN) of the SLD and the laser that we use in our experiment.

The motional dynamics of a levitated particle can be described by the Langevin equation

$$\frac{d^2 R^q}{dt^2} + \gamma^q \frac{dR^q}{dt} + \omega_q^2 R^q = \frac{f^q(t) + f_n^q(t)}{M}, \quad (1)$$

where R^q is the displacement along the axis q with q being the translational axis x , y , or z . $f^q(t)$ is a zero mean Gaussian process with an autocorrelation $\langle f^q(t) f^q(t + \tau) \rangle = 2Mk_B(\gamma_g T_g + \gamma_{ph}^q T_{ph}^q) \delta(\tau)$ and the total damping rate is $\gamma^q = \gamma_g + \gamma_{fb}^q + \gamma_{ph}^q$. The particle has mass M and oscillation frequency ω_q . The damping rate due to the gas molecules at a temperature T_g is γ_g while γ_{ph}^q and T_{ph}^q are the damping rate and temperature of the photon bath [6,16,20]. Due to the directional nature of photon scattering, γ_{ph}^q is axis dependent [20,21]. The damping exerted by the feedback is given by γ_{fb}^q . Additional heating effects [22] due to classical intensity noise and beam pointing fluctuations are captured in $f_n^q(t)$. Figure 1(c) shows the relative intensity noise (RIN) of our SLD and laser as a function of frequency. Between 30 kHz and 200 kHz, where we perform our reheating measurements, our SLD has a RIN between -131 dB/Hz and -135 dB/Hz and the laser has a RIN between -133 dB/Hz and -136 dB/Hz [5,14]. The reheating rate of the center-of-mass (CM) motion due to RIN depends on the trap frequency and the CM temperature of the oscillator while that due to the beam pointing instabilities depends only on ω_q [22]. Overall, the heating rate due to $f_n^q(t)$ is negligible, as we show below.

The fluctuation in the number of photons that interacts with the particle leads to CM heating much like the heating due to the fluctuating force originating from the gas molecules [16,18]. Energy gained by the particle per photon scattering event along direction q is $\delta E^q = \frac{\hbar^2 k^2}{2M} (k_i^q + k_s^q)^2$, where $k = \omega/c$. $k_i^q = [\sin \theta_i \cos \phi_i \sin \theta_i \sin \phi_i \cos \theta_i]$ and $k_s^q = [\sin \theta_s \cos \phi_s \sin \theta_s \sin \phi_s \cos \theta_s]$ are the projections of the unit vectors parallel to the incident (k_i) and the scattered (k_s) photons on the three translational axes with θ_i (θ_s) and ϕ_i (ϕ_s) the polar and azimuthal angle of the incident (scattered) photons. The variance of the photon number in a mode [18] is $\Delta N^2 = G(\omega) A_{pm} c M_d \Delta n^2$. The total energy gained [6,16,18] by the particle of polarizability α and scattering cross section $\sigma_s = \frac{\alpha^2 \omega^4}{6\pi \epsilon_0^2 c^4}$ due to the fluctuation in the photon number along q is

$$\begin{aligned} \frac{dE}{dt} \Big|_{ph}^q &= \int_0^\pi \int_0^{2\pi} \int_0^{\theta_{mx}} \int_0^{2\pi} \int_{\omega_c}^\infty \frac{P_r \sigma_s \Delta N^2 \delta E^q}{\Omega_{mx} A_w} d\omega d\Omega_i d\Omega_s, \\ &\approx \gamma_{ph}^q k_B T, \end{aligned} \quad (2)$$

where A_w is the cross-sectional area of the trapping beam at the focus, $d\omega_q = \sin \theta_i d\phi_i d\theta_i$, $d\Omega_s = \sin \theta_s d\phi_s d\theta_s$, and $P_r = \frac{3}{8\pi} (\cos^2 \theta_s \cos^2 \phi_s + \sin^2 \phi_s)$ is the spatial distribution of the scattered photons [21]. $\Omega_{mx} = 2\pi(1 - \cos \theta_{mx})$ is the solid angle formed by an incident photon with θ_{mx} being the largest angle between the wave vector of an incident photon and the z axis. We take $\theta_{mx} = 0.43$ rad, equivalent to an angle that a light ray makes at the full width half maximum of the Gaussian beam when focused using a high NA lens. $\gamma_{ph}^q = \Lambda^q \frac{\sigma_s I}{Mc^2} \frac{\hbar \omega_c}{k_B T}$ with $\Lambda^q = [0.12 \ 0.22 \ 0.65]$, where I is the intensity of the trapping light at the focus. To obtain an approximate analytical solution to compare with the recoil heating from a laser we initially set $G(\omega)$ constant. Note that the value calculated by numerical simulations performed using the exact profile $G(\omega)$ of the SLD are $\approx 10\%$ different. The frequency of the lowest-energy photon in the SLD emission spectrum is ω_c [$\lambda_c = 2\pi c/\omega_c \approx 1090$ nm, see Fig. 1(b)] while σ_c is the scattering cross section of the particle at ω_c . Note that Eq. (2) provides the standard recoil heating rates [21] when the laser variance of $\Delta N^2 = \bar{N}$ is used instead of that of the SLD, where \bar{N} is the average number of photons in the laser beam. For example, for a monochromatic laser of frequency ω , in the plane-wave case where $\theta_{mx} = 0$, Eq. (2) gives the recoil heating rate as derived by Seberson *et al.* [21] given in the x , y , and z directions by [127] $\frac{\hbar \omega \sigma_i I}{10Mc^2}$, respectively.

We measure the heating rate of the optically trapped nanoparticles by first cooling [10,23,24] the particle in a high vacuum ($\gamma_g < \gamma_{ph}^q$) and then turning off the feedback cooling ($\gamma_{fb} = 0$) allowing it to heat up. The evolution of the particle's energy [22,25] is

$$\begin{aligned} E_{cm}^q(t) &= \frac{\dot{E}_{bp}^q + E_\infty^q \gamma^q}{\gamma^q - \gamma_{rin}^q} \\ &+ \left(E_i^q - \frac{\dot{E}_{bp}^q + E_\infty^q \gamma^q}{\gamma^q - \gamma_{rin}^q} \right) e^{-t(\gamma^q - \gamma_{rin}^q)}, \end{aligned} \quad (3)$$

where E_i^q is the initial energy of the particle. The heating rate due to the beam pointing instability is \dot{E}_{bp}^q and γ_{rin}^q is

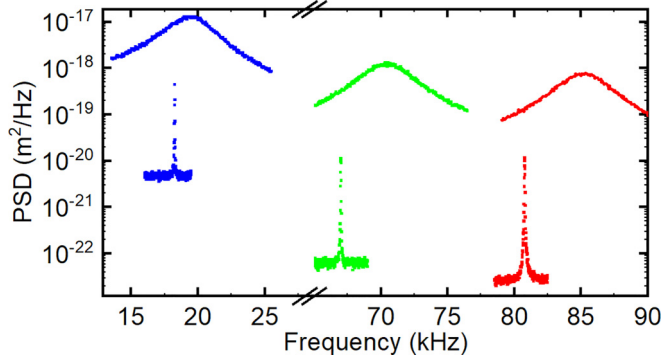


FIG. 2. Position power spectral densities (PSDs) of a 55 ± 16 nm radius silica nanosphere levitated using a SLD. The trapping power at the focus was 130 mW. The top graphs show PSDs at 5 mbar while the bottom graphs are the PSDs at 5×10^{-8} mbar when the particle is parametrically feedback cooled.

associated with RIN (see Appendix). The equilibrium energy of the particle, when no other heating mechanism, e.g., RIN is present, is $E_{\infty}^q = k_B(T_{\text{ph}}^q \gamma_{\text{ph}}^q + T_g \gamma_g) / 2\gamma_q$. The reheating time is typically very long (1000's of seconds), and as levitated particles are extremely sensitive to noise, a prolonged measurement time is generally not feasible. We instead perform the experiment within the linear regime [5] of the evolution process, i.e., $t \ll 2\pi / (\gamma^q - \gamma_{\text{rin}}^q)$, where we have the center-of-mass energy $E_{\text{cm}}^q(t) \approx E_i^q + E_{\infty}^q \gamma^q t$.

IV. RESULTS

Figure 2 shows the position power spectral densities (PSDs) of a SLD levitated 55 ± 16 nm particle at 5 mBar and at 5×10^{-8} mBar when it is parametrically feedback cooled. The particle size is obtained from the linewidth of the position PSD at 5 mBar. The uncertainty in the particle size arises from the 30% uncertainty in our measurement of pressure. At the lowest pressure the CM temperatures were 55 mK, 22 mK, and 45 mK along the x (polarization axis), y (orthogonal to the light field polarization), and z (trapping field propagation direction) axes, respectively. Once the lowest temperature is reached, the parametric feedback is switched off and the particle's dynamics are monitored as a function of time. After 150 ms, feedback is reactivated and the particle is again feedback cooled. Parametric feedback cooling is again switched off allowing the particle to reheat. This process is repeated 600 times and the averaged results are shown in Fig. 3(a), where we used $T_{\text{cm}}^q(t) = 2E_{\text{cm}}^q(t)/k_B$. We determine the energy of the particle using $E_{\text{cm}}^q(t) = M\omega_q^2 \langle q(t)^2 \rangle / 2$. The solid lines in Fig. 3(a) are fits of the form $a_0^q + a_1^q t$. The derived a_1^q is the sum of the reheating rates due to the gas molecules and that due to photons. The rate of increase of T_{cm} along the y and z axes are approximately equal and are significantly higher than that along the x axis.

Figure 3(b) represents plots of reheating rates of the particle as a function of residual gas pressure. As the gas pressure increases, the directional dependence of the reheating rates diminishes and eventually becomes negligible at a pressure of 2×10^{-6} mBar as the heating rate due to the gas molecules dominates those due to all other sources of heating. We fit a

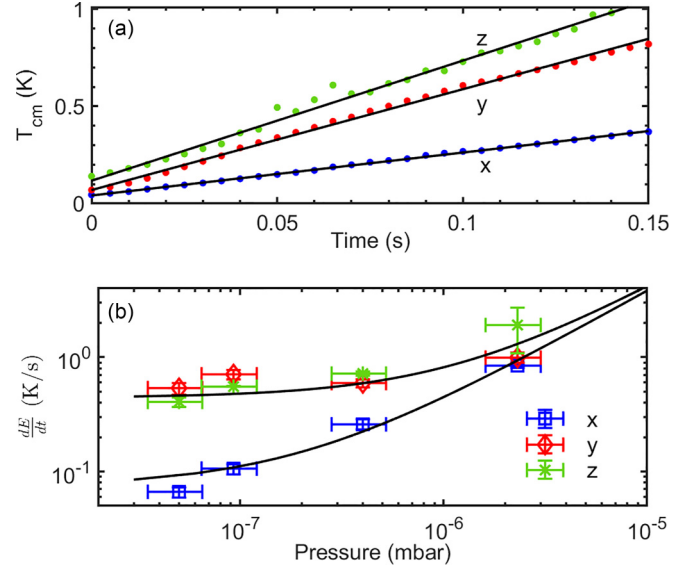


FIG. 3. (a) The evolution of the center-of-mass temperature of a $r = 55 \pm 12$ nm radius silica nanoparticle at 4×10^{-7} mbar after parametric feedback is switched off at time zero. This particle was levitated using the SLD. Each data point is the average of 600 time traces. The x axis represents the direction parallel to the light field polarization direction while the y axis is orthogonal to the light field polarization direction. The z axis is the propagation direction of the trapping light beam. Solid lines represent lines of the form $a_0 + a_1^q t$, where t denotes time, a_0 is the offset, and a_1^q is the reheating rate. (b) Reheating rates as functions of gas pressure. Solid lines represent $a_{\text{ph}}^q + a_2 P_g$, where a_{ph}^q is the heating rate due to the recoil of photons along the axis q , P_g is the gas pressure inside the vacuum chamber, and a_2 is a proportionality constant.

function of the form $a_{\text{ph}}^q + a_2 P_g$ to the reheating rates, where P_g is the gas pressure, a_{ph}^q is the reheating rate due to the photon recoil [Eq. (2)], and a_2 is the heating rate due to the gas molecules. We fit one line for the x direction and one for y and z axes which have similar values. The recoil heating rates given by the fits are $a_{\text{ph}}^x = 0.08 \pm 0.01$ K/s along the x axis and $a_{\text{ph}}^{y,z} = 0.45 \pm 0.07$ K/s along the y and z axes. From the fit we retrieve a reheating rate ($a_2 P_g$) of 0.018 ± 0.006 K/s due to the gas molecules at $P_g = 5 \times 10^{-8}$ mBar. This is consistent with that calculated for a particle of radius 55 nm. The theoretical photonic recoil heating rates [Eq. (2)] are 0.07 ± 0.05 K/s, 0.15 ± 0.13 K/s, 0.44 ± 0.39 K/s along the x , y , and z axes, respectively. The error bars arise from the systematic uncertainty in the particle size. The values for the x and z axes agree within the uncertainty of each measurement, but the heating rate in the y direction is higher than expected. To calculate the theoretical values we used a trapping power of 130 mW at the focus and $2\pi \hbar c / \mu_c = 1115$ nm (the band gap of the p - n junction). The relatively good agreement between the calculated and experimentally derived values for the x and z axes indicates that the heating rates at low pressures in these axes are dominated by the recoil of thermal photons. The reheating rates [22] due to RIN at 5×10^{-8} mBar were calculated to be 4.33×10^{-5} K/s, 2.48×10^{-5} K/s, and 2.81×10^{-6} K/s along the x , y , and z axes, respectively. These are about 1.89×10^3 , 1.82×10^4 , 1.60×10^5 times lower than

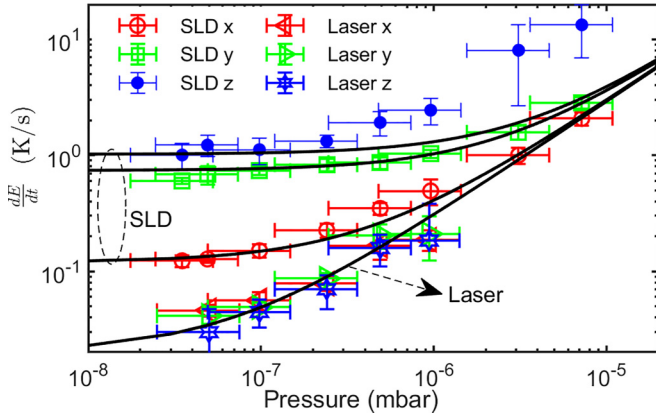


FIG. 4. Reheating rates of a $r = 70 \pm 20$ nm radius silica nanoparticle. This particle was initially trapped using the SLD beam and data on the reheating rates (top three data sets) at different gas pressures were collected. Subsequently, the particle was transferred to the laser beam and the reheating rates (bottom three data sets) at different gas pressure were recorded. The trapping laser power at the focus was 105 mW. Solid black lines represent fits of the form $a_{\text{ph}}^q + a_g P_g$.

$a_{\text{ph}}^{x,y,z}$ found above. Likewise, we find that the heating rates due to the beam pointing instability are orders of magnitude smaller than the recoil heating rates.

The axial variation of the heating rate results from the directional nature of the incoming field and the dipolar radiation pattern of the scattered field. Although the recoil heating from a thermal source is significantly larger than that from a laser, the ratio of these heating rates are only dependent on the spatial distribution of the incident and the scattered fields. In the Rayleigh limit, for a laser at 1064 nm, the ratios of these heating rates were calculated to be [1, 2, 7] for a plane wave (normalized by the x -axis value) and [1.0, 1.7, 4.6] when focused using a $\text{NA} = 0.77$ lens [21]. We consider only the Rayleigh regime in our calculation and obtain the same ratios as calculated for the laser for plane-wave illumination and [1.0, 1.81, 5.4] for the focused beam using our simple model. The measured ratio of the heating rates are [1, 5.6, 5.6] which, within the uncertainty of our measurements, are consistent with the predictions in the x and z directions, but are not in agreement for the y axis which indicates that there is again likely to be some excess heating on this axis.

We now present measurements of heating rates on a larger (radius $r = 70 \pm 20$ nm) particle levitated either by the SLD or the laser. To make these measurements the particle was transferred between the laser and the SLD traps [10]. At any time only one light beam is used for trapping. For this larger particle the recoil heating rates are larger than those of the 55 nm particle as the scattering cross section scales as r^6 . The gas damping has a smaller effect as it scales with radius as r^{-1} . Figure 4 shows plots of the reheating rates of this larger particle under the SLD and the laser levitation as a function of the residual gas pressure. Parametric feedback cooling along the z axis was not as efficient as for the 55 nm particle and the lowest CM temperature on this axis was ≈ 1 K. This meant that the particle was more susceptible to heating from parametric noise along this axis [5].

Like the smaller particle, the reheating rates of this larger particle also show a directional dependence which reduces with the increasing gas pressure as heating from gas collisions dominates. For this larger particle, the pressure at which the gas heating rate exceeds the recoil heating rates is approximately 7×10^{-6} mBar. This is about three times higher than that for the 55 nm particle and consistent with the reheating rates expected from gas damping. From fits to the SLD data we determine experimental recoil heating rates of 0.12 ± 0.02 K/s, 0.74 ± 0.07 K/s, 1.03 ± 0.25 K/s along the x , y , and z directions. From Eq. (2), the theoretical heating rates are 0.12 ± 0.10 K/s, 0.31 ± 0.26 K/s, and 0.90 ± 0.78 K/s along the x , y , and z axes, respectively. Again the experimental heating rates are consistent with the theoretical values along the x and z axes but not in the y axis. Moreover, these rates are twice as large as those of 55 nm particle and agree, within the uncertainty, with the values determined by the spheres radii. The experimental gas heating rate found from the fit is 0.014 ± 0.004 K/s at 5×10^{-8} mBar. This is again inline with the damping rate of particles of these size. The expected heating rates due to the laser are almost an order of magnitude lower than those due to the SLD. As evident in Fig. 4, we do not observe any directional laser heating in our experiment. We fit only one line and retrieve a small offset of 0.02 ± 0.01 K/s. This is comparable to the heating rate due to the gas molecules at 5×10^{-8} mBar. In the Rayleigh approximation [21], the recoil heating rates due to the laser are $\frac{dE}{dt}|_{\text{ph}}^x = 0.018 \pm 0.009$ K/s, $\frac{dE}{dt}|_{\text{ph}}^y = 0.036 \pm 0.030$ K/s, $\frac{dE}{dt}|_{\text{ph}}^z = 0.124 \pm 0.095$ K/s. Given we do not measure any axial dependence in the laser-induced reheating rates, deviation between the theoretical and experimental values is not unusual. Discrepancies may also arise from the approximations, e.g., Rayleigh scattering was made [21]. Similar deviations from the theory were recorded in other experiments when such a heating rate along one axis was measured using a laser [5,26].

V. DISCUSSION

If the particle can be held at lower pressures, where gas heating is not significant and where other sources of heating are not important, the particle should come to an equilibrium temperature determined by the thermal light, in this case the bulk temperature of the SLD [6,16]. Damping of the particle motion occurs via the Doppler effect. For a thermal light source at temperature T , the Doppler effect can be represented by an effective temperature [27] $T/(1 + \beta_{i,s})$ with $\beta_i = \mathbf{v} \cdot \mathbf{k}_i/c$, $\beta_s = \mathbf{v} \cdot \mathbf{k}_s/c$ and \mathbf{v} is the velocity of the particle. The damping force [6,27] is

$$F^q = \int_0^\pi \int_0^{2\pi} \int_0^{\theta_{\text{max}}} \int_0^{2\pi} \int_{\omega_c}^\infty \frac{P_r \sigma_s \hbar k (N_i k_i^q + N_s k_s^q)}{\Omega_{\text{mx}} A_w} d\omega d\Omega_i d\Omega_s, \\ \approx 2M\gamma_{\text{ph}}^q v^q, \quad (4)$$

where N_i and N_s are the photon numbers given by $\frac{GA_{\text{pn}} c M_d}{\exp[\frac{\hbar\omega(1+\beta_i)-\mu c}{k_B T}]-1}$ and $\frac{GA_{\text{pn}} c M_d}{\exp[\frac{\hbar\omega(1+\beta_s)-\mu c}{k_B T}]-1}$, respectively. At equilibrium the loss and gain in energy must be equal [6], e.g., $F^q v^q = \frac{dE}{dt}|_{\text{ph}}^q$, where $v_q^2 = k_B T_{\text{ph}}^q/M$. This implies $T_{\text{ph}}^q = \frac{T}{6}$. That is the motional temperature of the particle thermal-

izes within a factor of the bulk temperature of the photon source. The equilibration time $2\pi/\gamma_{\text{ph}}^z$ along the z axis for a 70 nm radius particle is ≈ 2000 s. To reach equilibrium, however, other sources of heating such as vibrations and parametric heating which become more important at higher temperatures need to be minimized.

VI. CONCLUSIONS

In conclusion, we demonstrated the enhanced recoil heating of a levitated optomechanical object due to thermal photons obtained from a superluminescent diode. This heating process dominates over other sources of heating such as the relative intensity noise and pointing instabilities. We measured the photonic heating rates along the all three trap axes for two sizes of nanoparticles. Future experiments could seek to measure the equilibrium temperature of a levitated particle in the photon-dominated regime in a deep trap. Here, one can consider ion or Paul traps for levitation, which are significantly deeper than the tweezer trap used here and are capable of levitating particles in a high vacuum without feedback cooling. In this case, the center-of-mass temperature of such an oscillator should thermalize with the bulk temperature of the photon source as envisioned by Einstein. Bose-Einstein condensates of photons [7,8] and thermalized photon gases [19] which have well-defined thermodynamic temperatures can potentially be used to control the center-of-mass temperature of such oscillators.

APPENDIX A: PHOTON STATISTICS OF AMPLIFIED SPONTANEOUS EMISSION

The Bose-Einstein (BE) distribution [28] is given by

$$P(n) = \frac{\bar{n}^n}{(1 + \bar{n})^{n+1}}, \quad (\text{A1})$$

where $\bar{n}(\omega) = 1/(\exp[(\hbar\omega)/(k_B T)] - 1)$ is the mean photon number in a mode. The variance of the photon number of a general BE distribution is given by $\Delta n^2 = \bar{n} + \bar{n}^2$. For a p - n junction, the average photon number in a mode is modified by the inclusion of a chemical potential μ_c or the band gap of the underlying p - n junction, i.e., $\bar{n}(\omega) =$

$1/(\exp[(\hbar\omega - \mu_c)/(k_B T)] - 1)$ [12]. For the blackbody radiation and similarly for the emission from a biased p - n junction [12], the degeneracy factor of a mode is given by $\frac{\omega^2}{\pi^2 c^3}$. As a result, the mean photon number and the variance of our thermal source (SLD) per meter cube per hertz [18] before amplification are $n_{\text{th}} = \frac{\omega^2}{\pi^2 c^3} \bar{n}$ and $\Delta n_{\text{th}}^2 = \frac{\omega^2}{\pi^2 c^3} \Delta n^2$. From a p - n junction photons are emitted via a surface area of A_{pn} . Moreover, in a SLD the output of a p - n junction is amplified using a single pass waveguide amplifier with a gain profile $G(\omega)$. Thus the overall mean photon number and the variance in time Δt are $G(\omega)c\Delta t A_{pn} n_{\text{th}}$ and $G(\omega)c\Delta t A_{pn} \Delta n_{\text{th}}^2$. Explicitly, the variance and the mean photon number per second per meter square are

$$\begin{aligned} N(\omega) &= G(\omega)cA_{pn}n_{\text{th}} \\ &= \frac{G(\omega)A_{pn}\omega^2}{\pi^2 c^2} \frac{1}{\exp[(\hbar\omega - \mu_c)/k_B T] - 1}, \quad (\text{A2}) \end{aligned}$$

$$\begin{aligned} \Delta N^2(\omega) &= G(\omega)cA_{pn}\Delta n_{\text{th}}^2 \\ &= \frac{G(\omega)A_{pn}\omega^2}{\pi^2 c^2} \frac{\exp[(\hbar\omega - \mu_c)/k_B T]}{[\exp[(\hbar\omega - \mu_c)/k_B T] - 1]^2}. \quad (\text{A3}) \end{aligned}$$

APPENDIX B: OUTPUT POWER OF A SUPERLUMINESCENT DIODE

The output power from a SLD with an effective surface area A_{pn} can be expressed as

$$\begin{aligned} P &= \int_{\omega_c}^{\infty} N(\omega)\hbar\omega d\omega \\ &= \int_{\omega_c}^{\infty} G(\omega)cA_{pn}n_{\text{th}}\hbar\omega d\omega \\ &= \int_{\omega_c}^{\infty} \frac{\hbar\omega^3}{\pi^2 c^2} \frac{A_{pn}G(\omega)d\omega}{\exp[(\hbar\omega - \mu_c)/k_B T] - 1}. \quad (\text{B1}) \end{aligned}$$

Even for a well behaved $G(\omega)$, e.g., the Gaussian-Lorentzian profile, Eq. (B1) does not have a closed form solution. For finding a closed form solution, we expand the denominator into a series taking into consideration the fact $(\hbar\omega - \mu_c) \gg k_B T$ and then perform integration assuming $G(\omega)$ is constant

$$\begin{aligned} P &= \int_{\omega_c}^{\infty} \frac{\hbar\omega^3}{\pi^2 c^2} \frac{A_{pn}G(\omega)d\omega}{\exp[(\hbar\omega - \mu_c)/k_B T] - 1} \\ &= A_{pn}G \int_{\omega_c}^{\infty} \frac{\hbar\omega^3}{\pi^2 c^2} [\exp[-(\hbar\omega - \mu_c)/k_B T] + \exp[-2(\hbar\omega - \mu_c)/k_B T] + \exp[-3(\hbar\omega - \mu_c)/k_B T] + \dots] d\omega \\ &\approx \frac{A_{pn}Gk_B T \omega_c^3}{\pi^2 c^2} \left[\exp[-(\hbar\omega - \mu_c)/k_B T] + \frac{1}{2} \exp[-2(\hbar\omega - \mu_c)/k_B T] + \frac{1}{3} \exp[-3(\hbar\omega - \mu_c)/k_B T] + \dots \right] \\ &\approx \frac{A_{pn}Gk_B T \omega_c^3}{\pi^2 c^2} \exp[-(\hbar\omega - \mu_c)/k_B T], \quad (\text{B2}) \end{aligned}$$

where in the third line we kept terms with ω_c^3 given $\omega_c^3 \gg \omega_c^2 \gg \omega_c$. In the last line we made the approximation $\exp[-(\hbar\omega - \mu_c)/(k_B T)] \gg \exp[-2(\hbar\omega - \mu_c)/(k_B T)]$.

From the manufacturer's specifications, we find the overall gain is ≈ 30 dB while from our measurement [see Fig. 1(b), the main text] we know $2\pi c/\omega_c \approx 1090$ nm. The manufacturer

does not provide any information about the chemical potential (band gap of the the p - n junction) and the area of the p - n junction. On the manufacturer's website (Innolume, GmBH) we find that they detect light up to about 1115 nm, although the intensity is about five orders of magnitude weaker than that at the peak. Based on this we use $hc/\mu_c = 1115$ nm in our calculation. Finally, to ensure that we obtain the measured power of $P \approx 130$ mW at the trapping location, we take $A_{pm} = 2.2 \mu\text{m} \times 2.2 \mu\text{m}$. Through the numerical integration

$$\begin{aligned} \left. \frac{dE}{dt} \right|_{\text{ph}}^q &= \int_0^\pi \int_0^{2\pi} \int_0^{\theta_{\text{mx}}} \int_0^{2\pi} \int_{\omega_c}^\infty \frac{P_r \sigma_s \Delta N \delta E^q}{\Omega_{\text{mx}} A_w} d\omega d\Omega_i d\Omega_s \\ &= \frac{A_{pm} G}{2MA_w \Omega_{\text{mx}}} \int_0^\pi \int_0^{2\pi} \int_0^{\theta_{\text{mx}}} \int_0^{2\pi} \int_{\omega_c}^\infty P_r \sigma_s \frac{\omega^2 \Delta n^2}{\pi^2 c^2} \hbar^2 k^2 (k_i^q + k_s^q)^2 d\omega d\Omega_i d\Omega_s \\ &= \frac{A_{pm} G}{2MA_w \Omega_{\text{mx}}} \int_0^\pi \int_0^{2\pi} \int_0^{\theta_{\text{mx}}} \int_0^{2\pi} \int_{\omega_c}^\infty P_r \sigma_s \frac{\omega^2}{\pi^2 c^2} \left[\frac{1}{\exp[(\hbar\omega - \mu_c)/k_B T] - 1} + \frac{1}{\exp[(\hbar\omega - \mu_c)/k_B T] - 1} \right] \\ &\quad \times \hbar^2 k^2 (k_i^q + k_s^q)^2 d\omega d\Omega_i d\Omega_s \\ &\approx \gamma_{\text{ph}}^q k_B T, \end{aligned} \tag{C1}$$

where, as in Eq. (B2), we expanded the exponentials in the third line and then performed integration and kept the highest order in ω_c , here ω_c^8 . Moreover, as in the main text, we have $\gamma_{\text{ph}}^q = \Lambda^q \frac{\sigma_s I \hbar \omega_c}{M c^2 k_B T}$, where $I = \frac{A_{pm} G \exp[(\mu_c - \hbar\omega_c)/k_B T] k_B T \omega_c^3}{A_w \pi^2 c^2}$. For θ_{mx} we used 0.43 rad. This is equivalent to an angle that a light ray makes at the full width half maximum of the Gaussian beam when focused using a high NA lens. From this expression we calculate heating rates due to recoil for the 55 nm particle in the x , y , and z axes as 8×10^{-2} K/s, 4.5×10^{-1} K/s, and 4.5×10^{-1} K/s.

APPENDIX D: HEATING DUE TO RELATIVE INTENSITY NOISE

The reheating rate due to the fluctuation in the intensity of the trapping light [22] is given by

$$\left. \frac{dE}{dt} \right|_{\text{RIN}}^q = \frac{\omega_q^2}{4} S_{\text{RIN}}(\omega_q/\pi) E_i^q, \tag{D1}$$

where ω_q is the trap frequency along the axis q , S_{RIN} is the spectral density of the relative intensity noise (RIN), $E_i^q = \frac{1}{2} k_B T_i^q$ is the initial energy of the particle before the parametric feedback is switched off, and T_i^q is the initial temperature. Since we measure heating rates at different pressure settings [see Figs. 3(a) and 4 in the main text], T_i^q , and thus E_i^q , depend on the pressure. At all pressure settings for which data were shown in Fig. 3(a), we have $T_i^q < 100$ mK along all axes. In the frequency range 35 kHz to 200 kHz, our SLD has [see Fig. 1(c), main text] has a relative intensity noise $S_{\text{RIN}} = -135$ dB Hz^{-1} which corresponds to $S_{\text{RIN}}(\omega_q/\pi) = 10^{-13.5} \text{Hz}^{-1}$. For the $r = 55 \pm 16$ nm particle in the main text, the trap frequencies in each direction are $\omega_x/2\pi = 71$ kHz, $\omega_y/2\pi = 85$ kHz, and $\omega_z/2\pi = 20$ kHz. At the lowest pressure of 5×10^{-8} mBar (Fig. 3(b), main text), the temperatures are $T_i^x = 55$ mK, $T_i^y = 22$ mK and $T_i^z = 45$ mK. We calculate $\left. \frac{dE}{dt} \right|_{\text{RIN}}^x = 4.33 \times 10^{-5}$ K/s,

of Eq. (B1) using the measured Gaussian profile, we obtain $P = 134$ mW.

APPENDIX C: HEATING DUE TO SCATTERING OF THERMAL PHOTONS

The gain in energy as specified in the main article is given [6,21]

$\left. \frac{dE}{dt} \right|_{\text{RIN}}^y = 2.48 \times 10^{-5}$ K/s and $\left. \frac{dE}{dt} \right|_{\text{RIN}}^z = 2.81 \times 10^{-6}$ K/s. For the 55 ± 16 nm particle (see the main text), these rates are about 10^3 – 10^5 times smaller than the heating rates due to thermal recoil.

APPENDIX E: HEATING DUE TO THE BEAM POINTING FLUCTUATIONS

The CM heating rate due to beam pointing instabilities from the light source and optical components was determined for atoms trapped in far off-resonant optical traps [22]. We used this expression, and measurement of the angular beam pointing instability of the SLD, just before the final focusing lens to estimate the displacement noise of the focused tweezer beam. The heating rate due to beam pointing instability is not dependent on the initial energy of the oscillator and is given by

$$\left. \frac{dE}{dt} \right|_{bp}^q = \frac{\pi}{2} M \omega_q^4 S_{bp}^q(\omega_q), \tag{E1}$$

where $S_{bp}^q(\omega_q)$ is the one-sided position spectral density arising from the fluctuation of the trapping beam's position and the other variables are defined above. We measure the pointing stability of the SLD beam in the focal plane using a quadrant photo diode which has the bandwidth required to measure fluctuations at twice the highest trap frequencies. The power spectral density associated with these beam fluctuations along each axis are determined by monitoring the difference signal in the horizontal (x axis) and vertical directions (y axis). To calibrate the difference signal from the quadrant photodiode we mount it on a translation stage and translate the diode along the x axis to record the difference signal as a function of displacement. For small displacements shown this is linear with a constant slope of $C_{bp} m/V$ for each axis. For the x axis, this constant is 1.17×10^{-4} m/V and a similar value of x is

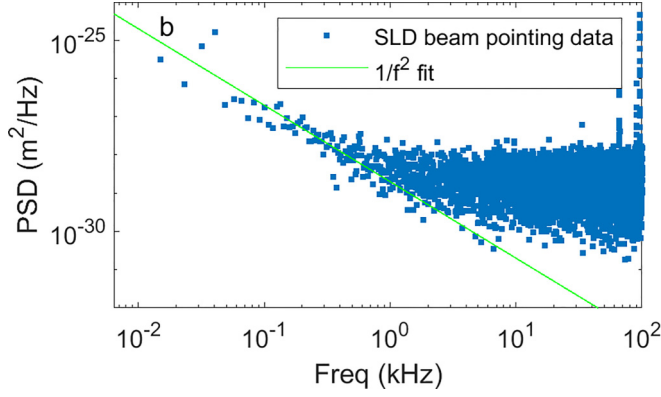


FIG. 5. Power spectral density associated with the SLD beam pointing instability along the x axis.

recorded in the y axis. To estimate the position fluctuation of the tightly focused trapping beam we assume that the predominant fluctuations are due to angular beam pointing instabilities. We convert the measurement of displacement to an angular beam pointing fluctuation given by $C_{bp}V/D$, where D is the distance from the last optical element before it is focused by the high NA lens. Finally, to determine the beam displacement at the beam focus we perform ray tracing calculations through the lens to find the focal displacement in the image plane for different input angles. This displacement is linear for small angular deviations of the beam and given by $\frac{dx}{d\theta} = 1.3 \times 10^{-3}$ m/rad. From the measurement of the beam pointing fluctuations we subsequently determine the position fluctuations at the focus by taking the PSD of the expression

$C_{bp}V/D\frac{dx}{d\theta}$ where V is the difference signal from each axis of the quadrant photodiode for $D = 2$ m.

Figure 5 is the plot of the fluctuations in the difference signal on the quadrant photodiode converted to position spectral density at the laser beam focus given by S_{bp}^q . At low frequencies up to approximately 10 kHz the PSD has a $1/f^2$ rolloff as shown by the fit, which is consistent with the displacement of mechanical components above resonance. These measurements and the rolloff are also consistent with relative measurements of position fluctuations made on the the advanced Laser Interferometer Gravitational-Wave Observatory (LIGO) laser system [29]. At the higher frequencies where our trap frequencies reside, the PSD is dominated by the RIN and the shot noise of the quadrant detector. The beam pointing stability cannot be directly measured, but we extrapolate the $1/f^2$ dependence measured at low frequencies up to 10 kHz to estimate the pointing stability. To estimate the heating due to beam pointing fluctuations we extrapolate the $1/f^2$ fit due to beam pointing stability to calculate S_{bp}^q at the x , y , and z trap frequencies given by 2.3×10^{-30} , 1.8×10^{-31} , and 1.3×10^{-31} . We calculate the heating rates due to the beam pointing instability using Eq. (E1) as $\frac{dE}{dt}|_{bp}^x = 1 \times 10^{-3}$ K/s, $\frac{dE}{dt}|_{bp}^y = 2 \times 10^{-3}$, and $\frac{dE}{dt}|_{bp}^z = 1 \times 10^{-4}$ K/s along the x , y , and z axes, respectively, which are more than two orders of magnitude smaller than the recoil heating rates.

APPENDIX F: EVOLUTION TOWARDS THE EQUILIBRIUM

With the feedback is of, f. i. e., $\gamma_{fb} = 0$, we have $\gamma^q = \gamma_{ph}^q + \gamma_g$ (see the main text). In this case, the rate of change of energy [22,25]

$$\begin{aligned}
 \frac{d\langle E^q \rangle}{dt} &= -\gamma^q \langle E^q \rangle + \gamma^q E_\infty^q + \dot{E}_{rin}^q + \dot{E}_{bp}^q \\
 &= -\gamma^q \langle E^q \rangle + \gamma^q E_\infty^q + \frac{\omega_q^2}{4} S_{rin}(\omega_q/\pi) \langle E^q \rangle + \frac{\pi}{2} M \omega_q^4 S_{bp}^q(\omega_q) \\
 &= -\gamma^q \langle E^q \rangle + \gamma^q E_\infty^q + \gamma_{rin}^q \langle E^q \rangle + \frac{\pi}{2} M \omega_q^4 S_{bp}^q(\omega_q) \\
 E^q(t) &= \frac{\frac{\pi}{2} M \omega_q^4 S_{bp}^q(\omega_q) + E_\infty^q \gamma^q}{\gamma^q - \gamma_{rin}^q} + \left[E_i^q - \frac{\frac{\pi}{2} M \omega_q^4 S_{bp}^q(\omega_q) + E_\infty^q \gamma^q}{\gamma^q - \gamma_{rin}^q} \right] \exp[-t(\gamma^q - \gamma_{rin}^q)] \\
 &\approx \frac{\frac{\pi}{2} M \omega_q^4 S_{bp}^q(\omega_q) + E_\infty^q \gamma^q}{\gamma^q - \gamma_{rin}^q} + \left[E_i^q - \frac{\frac{\pi}{2} M \omega_q^4 S_{bp}^q(\omega_q) + E_\infty^q \gamma^q}{\gamma^q - \gamma_{rin}^q} \right] [1 - t(\gamma^q - \gamma_{rin}^q)] \\
 &= E_i^q + \left[E_i^q (\gamma_{rin}^q - \gamma^q) + \frac{\pi}{2} M \omega_q^4 S_{bp}^q(\omega_q) + \gamma^q E_\infty^q \right] t,
 \end{aligned} \tag{F1}$$

where $\gamma_{rin}^q = \frac{\omega_q^2}{4} S_{rin}(\omega_q/\pi)$ and $E_\infty^q = k_B T_\infty^q / 2 = k_B (T_{ph}^q \gamma_{ph}^q + T_g \gamma_g) / 2 \gamma_q$ with $T_\infty^q = (T_{ph}^q \gamma_{ph}^q + T_g \gamma_g) / \gamma_q$ as defined in the main text. In arriving at Eq. (F1), we expanded the exponential when t is small. In our case, γ_{rin}^q and γ^q are comparable (see above). Moreover, $E_i^q \ll E_\infty^q$ and $\frac{\pi}{2} M \omega_q^4 S_{bp}^q(\omega_q) \ll \gamma^q E_\infty^q$,

consequently, as in the main text, we can write

$$\begin{aligned}
 E^q(t)^q &\approx E_i^q + \gamma^q E_\infty^q t, \\
 T(t)^q &= T_i^q + \gamma^q T_\infty^q t.
 \end{aligned} \tag{F2}$$

- [1] B. P. Abbott *et al.*, Observation Of Gravitational Waves From A Binary Black Hole Merger, *Phys. Rev. Lett.* **116**, 061102 (2016).
- [2] U. Delić, M. Reisenbauer, K. Dare, D. Grass, V. Vuletić, N. Kiesel, and M. Aspelmeyer, Cooling of a levitated nanoparticle to the motional quantum ground state, *Science* **367**, 892 (2020).
- [3] K. Murch, M. K., S. Gupta, and D. M. Stamper Kurn, Observation of quantum-measurement backaction with an ultracold atomic gas, *Nat. Phys.* **4**, 561 (2008).
- [4] T. P. Purdy, R. W. Peterson, and C. A. Regal, Observation of radiation pressure shot noise on a macroscopic object, *Science* **339**, 801 (2013).
- [5] V. Jain, J. Gieseler, C. Moritz, C. Dellago, R. Quidant, and L. Novotny, Direct Measurement Of Photon Recoil From A Levitated Nanoparticle, *Phys. Rev. Lett.* **116**, 243601 (2016).
- [6] A. T. M. Anishur Rahman and P. F. Barker, Realizing Einstein's Mirror: Optomechanical Damping With A Thermal Photon Gas, *Phys. Rev. Lett.* **127**, 213602 (2021).
- [7] J. Klaers, J. Schmitt, F. Vewinger, and M. Weitz, Bose–einstein condensation of photons in an optical microcavity, *Nature (London)* **468**, 545 (2010).
- [8] R. Weill, A. Bekker, B. Levit, and B. Fischer, Bose-einstein condensation of photons in an erbium-ytterbium co-doped fiber cavity, *Nat. Commun.* **10**, 747 (2019).
- [9] C. Gonzalez-Ballesteros, J. A. Zielinska, M. Rossi, A. Militaru, M. Frimmer, L. Novotny, P. Maurer, and O. Romero-Isart, Suppressing recoil heating in levitated optomechanics using squeezed light, [arXiv:2209.05858](https://arxiv.org/abs/2209.05858).
- [10] A. T. M. A. Rahman and P. F. Barker, Optical levitation using broadband light, *Optica* **7**, 906 (2020).
- [11] A. Smith, T. Easton, V. Guarrera, and G. Barontini, Generation of optical potentials for ultracold atoms using a superluminescent diode, *Phys. Rev. Res.* **3**, 033241 (2021).
- [12] P. Wurfel, The chemical potential of radiation, *J. Phys. C: Solid State Phys.* **15**, 3967 (1982).
- [13] C. Henry, Theory of spontaneous emission noise in open resonators and its application to lasers and optical amplifiers, *J. Light. Technol.* **4**, 288 (1986).
- [14] M. Blazek and W. Elsaesser, Emission state hierarchy governed coherence and intensity noise properties of quantum dot superluminescent diodes, *IEEE J. Quantum Electron.* **48**, 1578 (2012).
- [15] S. Hartmann and W. Elsaber, A novel semiconductor-based, fully incoherent amplified spontaneous emission light source for ghost imaging, *Sci. Rep.* **7**, 41866 (2017).
- [16] A. Einstein, On the present status of the radiation problem, *Phys. Z.* **10**, 185 (1909).
- [17] S. Hartmann, F. Friedrich, A. Molitor, M. Reichert, W. Elsässer, and R. Walser, Tailored quantum statistics from broadband states of light, *New J. Phys.* **17**, 043039 (2015).
- [18] M. Mansuripur and P. Han, Thermodynamics of radiation pressure and photon momentum, in *Optical Trapping and Optical Micromanipulation XIV*, edited by K. Dholakia and G. C. Spalding, International Society for Optics and Photonics (SPIE, New York, 2017), Vol. 10347, pp. 196–215.
- [19] J. Klaers, F. Vewinger, and M. Weitz, Thermalization of a two-dimensional photonic gas in a ‘white wall’ photon box, *Nat. Phys.* **6**, 512 (2010).
- [20] L. Novotny, Radiation damping of a polarizable particle, *Phys. Rev. A* **96**, 032108 (2017).
- [21] T. Seberson and F. Robicieux, Distribution of laser shot-noise energy delivered to a levitated nanoparticle, *Phys. Rev. A* **102**, 033505 (2020).
- [22] M. E. Gehm, K. M. O’Hara, T. A. Savard, and J. E. Thomas, Dynamics of noise-induced heating in atom traps, *Phys. Rev. A* **58**, 3914 (1998).
- [23] J. Gieseler, B. Deutsch, R. Quidant, and L. Novotny, Subkelvin Parametric Feedback Cooling Of A Laser-Trapped Nanoparticle, *Phys. Rev. Lett.* **109**, 103603 (2012).
- [24] J. Vovrosh, M. Rashid, D. Hempston, J. Bateman, M. Paternostro, and H. Ulbricht, Parametric feedback cooling of levitated optomechanics in a parabolic mirror trap, *J. Opt. Soc. Am. B* **34**, 1421 (2017).
- [25] Q. Long and Y. Wang, Effects of classical noises on atom cooling and trapping, *Phys. Lett. A* **288**, 257 (2001).
- [26] F. van der Laan, F. Tebbenjohanns, R. Reimann, J. Vijayan, L. Novotny, and M. Frimmer, Sub-Kelvin Feedback Cooling And Heating Dynamics Of An Optically Levitated Librator, *Phys. Rev. Lett.* **127**, 123605 (2021).
- [27] C. V. Heer and R. H. Kohl, Theory for the measurement of the earth’s velocity through the 3 K cosmic radiation, *Phys. Rev.* **174**, 1611 (1968).
- [28] M. Fox, *Quantum Optics: An Introduction* (Oxford University Press, New York, 2006).
- [29] P. Kwee, C. Bogan, K. Danzmann, M. Frede, H. Kim, P. King, J. Pöld, O. Puncken, R. L. Savage, F. Seifert, P. Wessels, L. Winkelmann, and B. Willke, Stabilized high-power laser system for the gravitational wave detector advanced ligo, *Opt. Express* **20**, 10617 (2012).